A Machine-Learning Approach for Classifying Defects on Tree Trunks using Terrestrial LiDAR

Van-Tho Nguyen, Thiéry Constant, Bertrand Kerautret, Isabelle Debled-Rennesson, Francis Colin

A Machine-Learning Approach for Classifying Defects on Tree Trunks using Terrestrial LiDAR

Van-Tho Nguyen[a], Thiéry Constant[a], Bertrand Kerautret[b], Isabelle Debled-Rennesson[c], Francis Colin[a]

[a] *Université de Lorraine, AgroParisTech, Inra, Silva, F-54000 Nancy, France*
[b] *Univ Lyon, Lyon 2, LIRIS, F-69676 Lyon, France*
[c] *Université de Lorraine, LORIA, UMR CNRS 7503, F-54506 Vandœuvre-lès-Nancy, France*

Abstract

Three-dimensional data are increasingly prevalent in forestry thanks to terrestrial LiDAR. This work assesses the feasibility for an automated recognition of the type of local defects present on the bark surface. These singularities are frequently external markers of inner defects affecting wood quality, and their type, size, and frequency are major components of grading rules. The proposed approach assigns previously detected abnormalities in the bark roughness to one of the defect types: branches, branch scars, epicormic shoots, burls, and smaller defects. Our machine learning approach is based on random forests using potential defects shape descriptors, including Hu invariant moments, dimensions, and species. The results of our experiments involving different French commercial species, oak, beech, fir, and pine showed that most defects were well classified with an average F_1 score of 0.86.

Keywords: roundwood quality, random forests, standing tree grading

1. Introduction

Grading standing trees and roundwoods is a critical task in a wood supply chain before harvesting or processing in the wood industry (Fonseca, 2005). This question is especially concerned by the general trend towards digitization for forest wood-chain traceability, supply chain optimization, and transformation (Pickens et al., 1997; Lin and Wang, 2012; Gardiner and Moore, 2014; Müller et al., 2019). After the overall shape characterization defining material yield, and wood quality information coming from the cross-sectional ends in the case of roundwood, wood quality is mainly assessed from singularities of the bark surface. The occurrence of such singularities indicates local variations of the material properties generally corresponding to decreased normal distribution of the clearwood properties and characteristics, which detrimentally impact future products and their mechanical, physical or aesthetical functions. Nevertheless, the resulting grade made by an expert corresponds to a global assessment of the quality by taking many criteria into account through grading rules. After the attribution of the grade, the original causes are often forgotten.

Alternatives using X-ray computed tomography (CT) can be considered as reference methods for such a characterization (Li et al., 1996; Zhu et al., 1996; Aguilera et al., 2008; Colin et al., 2010b). On the one hand, CT can achieve good accuracy for defect recognition (up to 95%; Li et al. (1996)), detect the defects as small as 1 millimeter in diameter by manually placing plot markers along the tracks of knot (Colin et al., 2010b), or automatically detect knots (Longuetaud et al., 2012; Krähenbühl et al., 2012, 2016). Industrial solutions are proposed by several companies (Microtec, 2019; Jörg

Elektronik GmbH, 2019). On the other hand, CT has its own limitations with investment cost and the need to fell the tree and cut it into logs. Besides the fact that grading rules are mainly defined from external observations where bark is present, recent studies confirmed a strong correlation between internal and external defects (Thomas, 2009; Stängle et al., 2014; Racko, 2013; Pyörälä et al., 2018) with coefficients of determination (R^2) greater than 0.6. From these results and practices, the question arose as to the use of three-dimensional (3D) technologies for describing the external envelope of trunks or logs with the objective of detecting bark surface defects.

LiDAR (Light Detection and Ranging) can measure objects in three dimensions through a technique in which a laser beam is emitted and the reflected light is received by a detector. The resulting product is a point cloud that contains the three spatial dimensions (x, y and z coordinates) of the scanned object. In forestry, terrestrial laser scanning (TLS) can provide information about an individual tree or a plot (Dassot et al., 2011). A variety of forestry applications have been developed in the last two decades. In particular, a number of studies has taken advantage of the potential of LiDAR for the replacement of conventional methods of measuring forest inventory parameters, such as tree height, diameter at breast height (DBH, trunk diameter measured at 1.3 m above ground level) (Hopkinson et al., 2004; Simonse et al., 2003), stand density, stand basal area, and volume for biomass assessment (Van Leeuwen and Nieuwenhuis, 2010; Yao et al., 2011; Dassot et al., 2012; Astrup et al., 2014).

On standing trees, there have been attempts to estimate tree quality criteria from TLS (Kankare et al., 2014; Blanchette et al., 2015), airborne

LiDAR (Maltamo et al., 2009; Luther et al., 2014; Kankare et al., 2014), or both types of LiDAR (Van Leeuwen et al., 2011). The quality parameters targeted in these works mainly concerned the overall shape of the timber: ovality, curvature, taper, and the presence of branches. Research focused on the detection of external defects are scarce (Schütt et al., 2004; Stängle et al., 2014; Thomas et al., 2007; Kretschmer et al., 2013). Most of these studies were dedicated to the detection of large and very obvious defects. Thomas et al. (2007); Thomas and Thomas (2010) detected, on red oak and yellow poplar, defects with a diameter greater than 7.5 cm and protruding by at least 2.2 cm from the bark. Kretschmer et al. (2013) proposed an approach to detect and manually measure the branch scars on Scots pine by highlighting them on a 3D reconstruction of the bark surface: the bark surface is colored based on the distance to a fitted cylinder surface corresponding to a trunk part. The scars, with a diameter of at least 2 cm and protruding by at least 1.5 cm from the bark, were detected. Existing research on the automated classification of defects on tree bark using TLS is even scarcer. Schütt et al. (2004) presented a semi-automatic approach, based on a neural network, to detect and classify wood defects using both range and intensity information of TLS data.

In a previous work (Nguyen et al., 2016b), we successfully developed an algorithm to detect the defects on trunks surface. Using a suitable spatial resolution of the 3D data, the detection can segment potential defects with a dimension as small as 1 cm and small protrusion on trunks of different tree species. This important improvement was obtained from two major components. First, the definition of the most relevant trunk centerline results from

a voting algorithm selecting the most frequent locations of the intersections of the inward pointing normals to the surface. Secondly, the reference distance to the centerline is computed for each individual point by taking its neighborhood into account. The computation of reference distance for each individual point allows for more precisely detecting the abnormalities on the bark than more global reference surface based on primitive fitting such as cylinder (Schütt et al., 2004; Stängle et al., 2014; Kretschmer et al., 2013) or circle (Thomas et al., 2007; Thomas and Thomas, 2010).

Returning to the main purpose of the work presented here, once potential defects are detected, an automatic procedure must be able to assign them to a defect type and to confirm their status. The main challenge in the classification of these defects is to deal with the variability of their appearance, even for the same type of defect. In the forestry domain, the defects are often defined by the biological origin (Colin et al., 2010a) that leads to a high intra-class variability and inter-class similarity. Figure 1 (c-f) and (g-i) give examples of the intra-class variability between branch scars and burls respectively. Inter-class similarity between an epicormic shoot and a burl is shown in Figure 1 (b) and (g). Factors contributing to the intra-class variability or inter-class similarity are the tree species, often linked to the characteristics of its bark, the shape and the age of the defect and all the history of its development in connection with the environment of the tree. Facing this huge variability, a major difficulty is to build a representative database allowing the establishment of classification methods and their testing especially in studying the feasibility of such an approach as in this work. Several methods in the field of pattern recognition can be applied

to classify objects, such as neural networks (Bishop, 1995), support vector machines (Cortes and Vapnik, 1995), random forests (Breiman, 2001), Bayes classifier (Devroye et al., 1996), and deformable models (Terzopoulos and Fleischer, 1988). Most approaches are based either on parametric models or on machine-learning techniques. In the remote sensing domain, the machine-learning supervised classifiers are widely used because they are more flexible in handling the high variability in object appearance and are more robust than model-based approaches (Niemeyer et al., 2014). In particular, random forests are a supervised machine-learning method that is based on ensembles of classification trees. Random forests exhibits many interesting properties, such as high accuracy, robustness against over-fitting, noise or missing data in the training set (Díaz-Uriarte and De Andres, 2006). Moreover, random forests is a non-parametric method that does not require the information on the distribution of data. These advantages make random forests a successful classification method since its introduction by Breiman (2001). In the domain of remote sensing, random forests were used in landcover classification or urban area classification from airborne LiDAR (Chehata et al., 2009; Guo et al., 2011) or Landsat data (Yuan et al., 2005; Gislason et al., 2006). In the forestry domain, random forests were used to accompany the forest inventory, such as for biomass assessments (Mutanga et al., 2012), using airborne LiDAR. Othmani et al. (2013) used random forests to identify the tree species from the analysis of tree bark pattern from the mesh derived from TLS data. Random forests were used to assess the timber quality of Scots pine by estimating tree properties, such as trunk diameters, tree height and branch heights using the parameters computed from TLS data (Kankare

et al., 2014).

The main objective of this work is to classify the potential defects detected on trunk surface by previously developed algorithms (Nguyen et al., 2016b). The other objective is to evaluate the performance of a robust and commonly used machine-learning algorithm, random forests, for the classification of bark singularities. The targeted types of defects are branch, branch scar, burl, and small defects including sphaeroblast, bud cluster, and picot. These types were chosen to represent the existing diversity of defects; nevertheless, some were grouped because of the difficulty in distinguishing them given their size or shape. We aimed to develop a method that works on the common commercial tree species, including hardwood species like sessile oak (*Quercus petraea* (Matt.) Liebl.), European beech (*Fagus sylvatica* L.), and wild cherry tree (*Prunus avium* (L.) L.), or conifers such as silver fir (*Abies alba* Mill.), Scots pine (*Pinus sylvestris* L.), and Norway spruce (*Picea abies* (L.) H.Karst.). Here a special focus is given to the results concerning oak and European beech two hardwood species that have very different bark roughness, defect types and shapes. The first species has a furrowed bark and its most common defect types are burl and picot. The second has smooth bark and the most common defect type is branch scar with an eyebrow (or "Chinese mustache") shape.

2. Materials and Methods

2.1. Defects on trunk surface

Several defects on the trunk surfaces can be caused by exogenous factors depending on their environment, such as heat, frost, other trees, animals, and

human beings. Our study focused on the most frequent source of defects, which arises from tree branching. Branching defects are the result of the development and growth of the tree. Their scars are associated generally with protruding regions that result from the inclusion of the defect by the radial growth of the trunk. More precise definitions of what we considered as a branching defect were as follows:

- A sequential branch was a branch that emerged after a winter's rest of the original bud.
- An epicormic branch was a branch that emerged after several winters from a latent bud.
- A branch scar was a track of a branch, either sequential or epicormic that maintains when this branch has died and has been degraded. Branch scars on hardwood were often referred to as bark distortions.
- A bud was a miniature leafy shoot protected by a covering of scales.
- A burl was a group of juxtapositional defects of one or more type, such as bud, picot, branch or branch scar. By definition, a burl could have a great variability in shape and size and composition.
- A bud cluster was a limited group of buds of less than six buds.
- A sphaeroblast was a bud whose base produces xylem that progressively covers the apical meristem of the bud (mainly on beech) (Fink, 1999).
- A picot was a small branch with its apex naturally pruned. Picots are defined and illustrated in Colin et al. (2010b).

Typical defects on trunk surface were represented in Figure 1. These defects were characterized by a large intra-class variability in size and shape. For instance, burls could range from a large bud cluster with at least six buds to a very extended mass of buds, picots, short or long branches with a diameter of several tens of centimeters.

The impact of defects on the wood quality depended on their type and dimension. For defects of the same type, larger defects had a more important impact than smaller ones. In general, the most penalizing defects were branch scar, branch and burls. The impact of small defects such as bud cluster, sphaeroblast and picot is small, but some had to be taken into account in the highest quality class.

2.2. Methodology

The steps of our method are presented in Figure 2. After their acquisition, the TLS data were preprocessed to obtain a smooth mesh corresponding to a trunk portion. Next, the potential defects were detected by using a segmentation algorithm, which is an improved version of the previously published work (Nguyen et al., 2016b) and is summarized in section 2.5. Then, the potential defects were classified into defect types using trained random forests. Finally, the results were visualized by various colors on the mesh according to the defect type. The classification was validated by comparing the results with the ground-truth labels classified by an expert on the trunks before the TLS scans were carried out. Two methods were used by the expert to mark the defect type. The first method used small distinctive shape pinned in the vicinity of the defect. Thus, the defect type was recognized in the reconstruction of trunk surface. The second method measured the coordi-

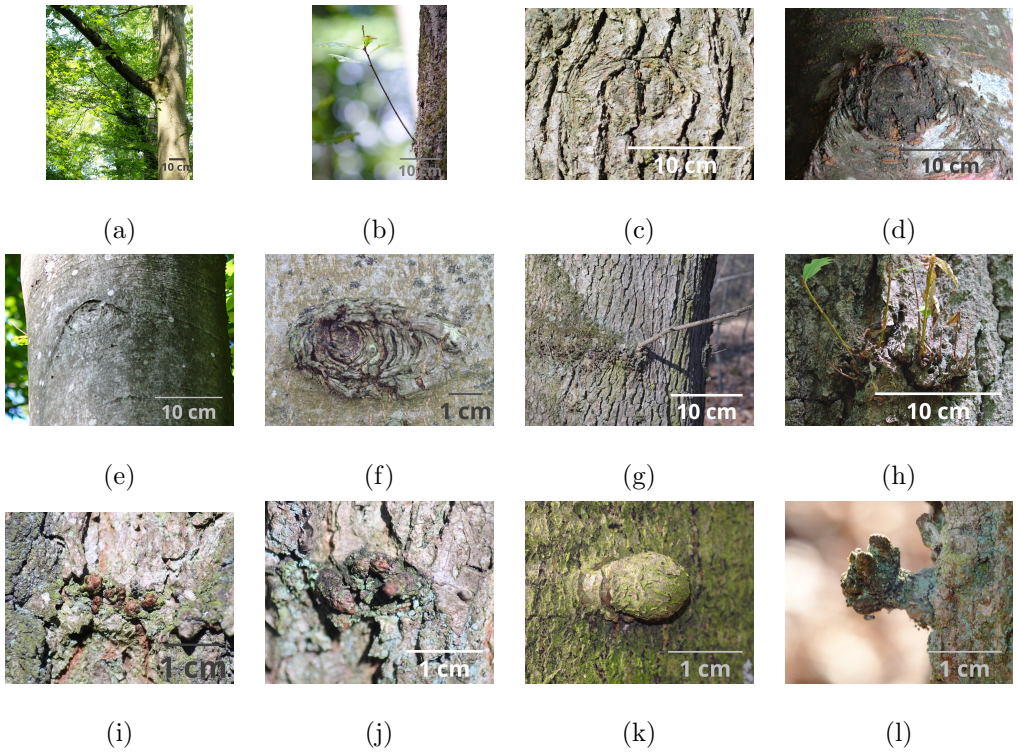

Figure 1: Some illustrations of the defect types considered in this study. (a, b) branches: sequential branch (a), and epicormic shoot (b); (c-f) branch scars: on oak (c), on wild cherry (d), on beech (e), and on beech (f); (g, h) burl: consisting of buds and an epicormic shoot (g), buds and short epicormic shoots (h), and buds (i); small defects: (j) bud cluster, (k) sphaeroblast, and (l) picot.

nates of the defects by a local coordinate (l, z) system on the trunk with l the position along a longitudinal axis Oz and l the signed arc length between the reference axis and the defect center. Two ping-pong balls were used to define the axis. A dedicated software was developed to recover the same coordinate system on the reconstruction of trunk surface, which allowed for measuring the defect coordinates and comparing with the ground truth. The

ground truth contained all of the defects with a diameter equal or greater than 0.5 centimeters and from 0.5 to 2 meters or 5 meters depending on the distribution of defects.

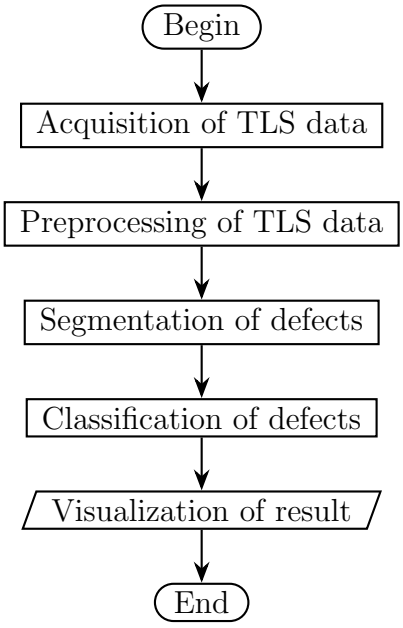

Figure 2: Overview of the processing flow for classifying the surface defects onto a trunk.

2.3. Acquisition of TLS data

The tree trunks exhibiting different defects were measured with a Faro Focus 3D X130 laser scanner in the Champenoux and Haye forests in the Grand-Est region of France. To detect small defects, we chose a high-resolution setting and put the scanner close to the trunk. The utilized resolution was one half of the maximum value and the distance from the scanner to the trunk was approximately 3-4 meters. With this setting, the angular resolution of the scan was 0.018° in both horizontal and vertical directions, and the resulting distance between two neighboring 3D points on the trunk surface in the

point cloud was around 1 millimeter. Such settings ensured a high-quality description of the defects limiting the laser beam inclination resulting from the defect height and the distance to the tree. The trees were sampled according to several criteria. Among the main commercial species, selected trees must have a sufficiently large diameter (see Table 1) and represent a variability in bark roughness, which depends on the species and the age of the trees. In agreement with these criteria, we scanned 26 trees: nine sessile oaks, eight European beeches, three wild cherries, two Scots pines, three silver firs, and one Norway spruce. These scans were divided into 2 sets. One was used to train the random forests and another was used to test the method efficiency (Table 1). The training set contained 425 defects from 16 trees and the test set contained 183 defects from 10 trees.

During this acquisition step, the objective was to maximize the number and type of defects per scan; thus, trunks were either scanned entirely with four scans from suitable points of view or partially with one or two scans on just one side. If the trunk was scanned from multiple points of view, the scans were merged into a single file per tree to recover the 3D view of the trunk. The registration was performed by the standard procedure available in the FARO SCENE software (Faro Technologies Inc., Lake Mary, FL), through the use of spheres.

2.4. Preprocessing of TLS data

LiDAR data are generally noisy, and the first processing step aimed to manage noise for enhancing the recognition rate. It included the reduction of noise and the smoothing of the trunk surface. Noise reduction is a difficult and complex process, due to different noise patterns from scan to scan. It

Table 1: Number and attributes of the sample trees.

Species	**Number of trees**		**Range of diameters**
	Training	**Testing**	**at breast height (cm)**
Oak	6	3	35 - 76
Beech	5	3	30 - 57
Wild cherry	2	1	22 - 33
Pine	1	1	34 - 57
Fir	2	1	23 - 45
Spruce	0	1	19
Total	16	10	

depends on the condition of the scanning environment and also the characteristics of the trees. For example, we observed that when the trunk had branches or small epicormic shoots, there was much of noise caused by the multiple interceptions of the same laser beam by several branches and the bark. This is the situation when a laser beam hits both the contour of the branch and the bark resulting in a ghost point, with no reality, between the branch and the bark (Figure 3 (a)). We observed that the point density in noisy regions was often lower than in the relevant data regions. Thus, we proposed a simple approach to remove noise by clustering the point cloud by Euclidean distance with the idea that relevant data points are in the largest cluster where the point density is highest. The choice of the threshold on the minimal distance between clusters is critical. If the threshold is too small, there is a risk that the relevant data would be removed, especially in the high part of the trunk where the resolution is lower. After testing different values,

we set the threshold to 5 millimeters, which gave the best visual results for our scanning settings.

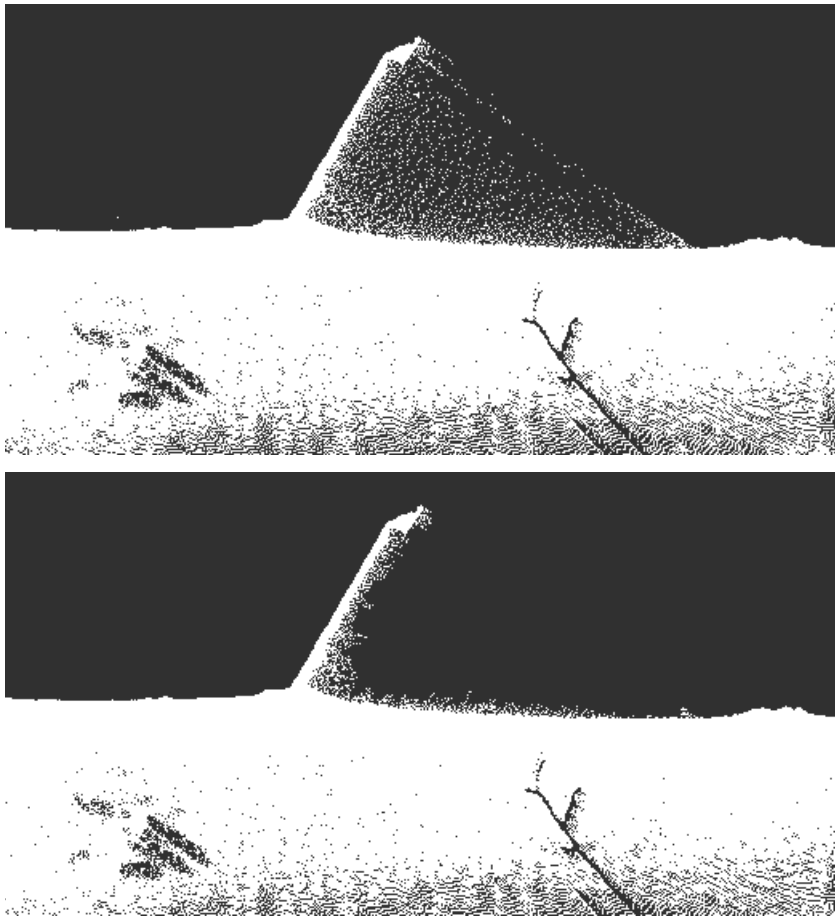

Figure 3: Noise processing for a wild cherry trunk. Point cloud before (a) and after (b) noise reduction process that only keeps the biggest cluster; the minimal distance between two clusters is 5 millimeters.

Due to the nature of a laser scan, the raw point cloud contains a certain level of error. For example, the utilized scanner had a ranging error of ± 2 millimeters at 10 meters. The smoothing step was performed

to reduce surface roughness caused by ranging uncertainty. However, the smoothing intensity was limited to maintain the bark roughness or defect shapes. The following steps were performed for smoothing and creating a mesh from the trunk point cloud using the Graphite software (`https://gforge.inria.fr/frs/?group_id=1465`):

1. Smooth the point cloud (Lévy and Bonneel, 2013) using only one iteration with 30 neighbors. Only one iteration was used because with more iterations the smoothing process may erase defects with a weak relief.
2. Reconstruct the trunk surface (Boltcheva and Lévy, 2017) with the normal vector computed from 30 neighbors and the maximum distance used to connect neighbors of 5 millimeters. The radius value was chosen to be greater than the between-point distance in the point cloud but not too large to prevent the creation of wrong edges.
3. Smooth the created mesh by using the remesh smooth function (Lévy and Bonneel, 2013). The used parameter was the number of points similar to the one of the original point cloud.

2.5. Segmentation of defects

Our strategy to classify the defects on trunk surface was first to detect all potentially defective areas using a segmentation algorithm. The algorithm is an enhanced version of our previously published one (Nguyen et al., 2016b) that focuses on defects with little protuberance from tree bark. In this study, we proposed a preliminary step for segmenting tree branches. The motivation for developing this approach came from the existing links between a defect

present in the woody part and the impact of that defect on the bark surface, expressed by a structured, and often protruding, irregularity. To detect these irregularities, we defined the centerline of the trunk as a reference. In the evaluation of the algorithm presented in Nguyen et al. (2016b), the presence of branches was identified as an inconvenience for detecting smaller defects in a branch vicinity. Thus, in this work, the branches were first segmented by an algorithm that separates the points into two disjointed sets (illustrated in Figure 4): (1) set T contains closer points to the trunk surface, and (2) set B contains the branches according to the following algorithm.

- Estimation of the trunk radius r_m, using the mode of the distance to the centerline of all points in the point cloud.

- Division of the point cloud volume into slices with a thickness of l millimeter, following the centerline direction. Each slice was then divided into angular sectors with an angle of $\frac{l}{r_m}$ radian. The value of l should be greater than the diameter of the largest branch. In our experiment, the l parameter was set to values between 50 and 100 millimeters.

- For each angular sector, the nearest point to the center of the trunk was added to set T, and the other points of the portion were added to set B.

- For each point P in set T, we found subset S of set B, such as the distance between point $S_i \in S$ and P was less than or equal to $\sqrt{2}l$, and we moved them in set T. This algorithm assured that no point on trunk surface left on the branches set B by accepting a branch part with a length of $\sqrt{2}l$ on the trunk set T.

After the branch segmentation, the original method (Nguyen et al., 2016b) was applied to set T as follows. (i) For each point P in set T, we estimated a reference point $\hat{P}$ from a linear regression linking the radius variation to longitudinal positions on a patch of neighboring points of P. (ii) The defect points were detected by thresholding the difference between the distance from P and $\hat{P}$, denoted as (δ). (iii) The threshold was automatically computed on the histogram of δ using the Rosin's method (Rosin, 2001). Then, the detected defect points were merged with set B containing the branches to form a set of defect points D. The different potential defects were obtained by clustering the defect points D by using Euclidean distance.

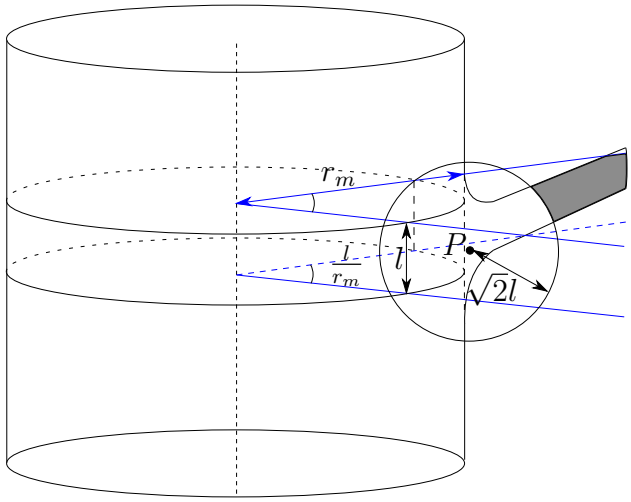

Figure 4: Illustration of the branch segmentation: the angular sector is defined by the volume inside planes formed by blue lines. The points in this angular sector that had a distance to P less than or equal to $\sqrt{2}l$ were moved to the set of trunk points (T). The set of branch points (B) is in solid grey color.

2.6. Classification of defects

2.6.1. The random forests classifier

The random forests (Breiman, 2001) classifier is an ensemble classifier that aggregates a set of classification and regression trees (CARTs) (Breiman et al., 1984) to make a prediction. In the training step, all trees were built with the same parameters but on different subsets of the training samples. These subsets were generated from the training samples by a bootstrap sampling, which randomly selected the same number of vectors from the original set. The remaining "out-of-bag" (OOB) was used to compute the estimation error, which is known as the OOB error. Unlike CART, random forests does not consider all variables at each node to determine the best split threshold but a random subset of variables of the feature vector and the trees are built without pruning. The cardinality of the subset is an input parameter.

Another important parameter of the random forests classifier is the number of trees, which must be sufficiently large to capture the full variability of the training data and yields good classification accuracy. One of the advantages of the random forests classifier is that it does not overfit when increasing the number of trees at the expense of slower running time. In the classification step, random forests tested the feature vector, describing the new object with each tree in the forest. Each tree made a classification, or in other words, gave a vote for a class. The random forests classifier chose the class on which the majority of trees voted.

As mentioned above, the number of trees in the forest ($nbTrees$) and the number of variables ($nbVariables$) used to select and test for the best split when growing the trees are two important input parameters needed to train

the random forests classifier. The OOB error can be used to find the optimal value for these parameters. We ran an experiment with the $nbTrees$ from 100 to 5,000 and the $nbVariables$ from 1 to the number of variables of the feature vector. For each value of $nbVariables$, we could find the minimum value of $nbTrees$, which gave the minimum OOB error.

The random forests has been implemented in a number of free and open source libraries. In this study, we used the implementation in OpenCV-3.3 (Bradski, 2000). The advantage of OpenCV is its compatibility with the implementation of our algorithms in C++ programming language. The source code and sample data are available at the following GitHub repository: `https://github.com/vanthonguyen/trunkdefectclassification`

2.6.2. Feature vector

In this step, we used the defects detected by our segmentation algorithm and constructed the feature vector based on our expertise on the defects. Before computing the features, the point cloud of the defect was converted from Cartesian coordinate system to a custom coordinate system $\{l, z, d\}$, where l is the arc length computed from angle between the point and the plane Oxz and the distance from the point to the centerline, z is the height, and d is the difference between the distance and the reference distance from the point to the centerline (the distance between P and $\hat{P}$ as presented in section 2.5). This conversion allowed us to measure the defect diameter along the curved surface of the trunk similar to a manual measurement. To reduce the inhomogeneity of point clouds due to the superimposition of data coming from several points of view or the non-uniform by TLS, the feature vector was computed from a subsampled point cloud. The subsampled point cloud

latter was computed by keeping only the closest point to the center of each voxel of a regular voxel grid of the defect point cloud. The voxel size was chosen by the average point spacing, which was 3 mm in our study. The following features were used:

1. Species: s.
2. Ratio between the number of points of the defect and the volume of its bounding box: c (equation 1)
3. Defect arc length: $w = l_{max} - l_{min}$.
4. Ratio between w and defect height: $\frac{w}{h}$ where h equals $z_{max} - z_{min}$.
5. Ratio between w and maximum of d: $\frac{w}{d_{max}}$.
6. Mean of difference between the distance from P and $\hat{P}$ for all points P of the defect: $\bar{d}$.
7. Standard deviation of the difference between the distance from P and $\hat{P}$ for all points P of the defect: σ_d.
8. Hu moment invariants: $I_1, I_2, I_3, I_4, I_5, I_6, I_7$ (see equations 4–10).
9. Ratio between the eigenvalue λ_1 and the eigenvalue λ_3: $\frac{\lambda_1}{\lambda_3}$.
10. Ratio between the eigenvalue λ_2 and the eigenvalue λ_3: $\frac{\lambda_2}{\lambda_3}$.
11. Angle between the eigenvector $\overrightarrow{v_3}$ and the trunk axis at the height of defect: α.

where λ_1 is the eigenvalue associated with the eigenvector $\overrightarrow{v_1}$ of the defect having the smallest angle, with the radial vector of the trunk at the center of the intersection between the defect and the trunk. λ_2 is the eigenvalue associated with the eigenvector $\overrightarrow{v_2}$ of the defect having the smallest angle with the tangential vector of the trunk at the center of the intersection between

the defect and the trunk. λ_3 is the eigenvalue associated with the eigenvector $\overrightarrow{v_3}$ of the defect having the smallest angle with the trunk axis at the height of defect.

The species was an important variable because each one had a specific bark roughness and a set of defects. For example, oak had burls but does not had sphaeroblast, which was conversely related to beech. In addition, for the same defect type, its shape could differ from one species to another. For example, a branch scar on oak and on beech was very different.

Another relevant variable was the ratio between the number of points of the defect and the volume of its bounding box, which measured the compactness of the defect in the $\{l, z, d\}$ coordinate system equation (1). This feature could discriminate a flat defect and a significantly protruding defect.

$$c = \frac{number\ of\ points}{(l_{max} - l_{min})(z_{max} - z_{min})(d_{max} - d_{min})} \tag{1}$$

By using our expertise in the domain, the dimension was an important criterion to classify defects, in particular small defects such as small burl and bud cluster. For that reason, we included the arc length w as a feature. The ratio $\frac{w}{h}$ allowed us to distinguish between a branch scar and a bark zone, which had a roughness higher than the local average on oak tree because the branch scars often have width greater than height and bark zones have width smaller than height. The ratio $\frac{w}{d_{max}}$ helped to distinguish a flat object, such as bark portion, branch scar and a more protruding one such as sphaeroblast and picot. The mean and standard deviation of d were also included in the feature vector because they help to distinguish between a branch scar and a burl composed only of buds.

The Hu moment invariants (Hu, 1962) had good characteristics for the object recognition because they were invariant with respect to translation, scale, and rotation. The Hu moment invariants $\{I_1, \ldots, I_7\}$ were computed from the normalized central moments nu_{ij} of orders (i + j) 2 and 3 (see equations (3)–(10)).

$$mu_{ij} = \sum_{z,l} (z - \bar{z})^i (l - \bar{l})^j d \tag{2}$$

$$nu_{ij} = \frac{mu_{ij}}{mu_{00}^{(i+j)/2+1}} \tag{3}$$

$$I_1 = nu_{20} + nu_{02} \tag{4}$$

$$I_2 = (nu_{20} - nu_{02})^2 + 4nu_{11}^2 \tag{5}$$

$$I_3 = (nu_{30} - 3nu_{12})^2 + (3nu_{21} - nu_{03})^2 \tag{6}$$

$$I_4 = (nu_{30} + nu_{12})^2 + (nu_{21} + nu_{03})^2 \tag{7}$$

$$\begin{aligned} I_5 = (nu_{30} - 3nu_{12})(nu_{30} + nu_{12})[(nu_{30} + nu_{12})^2 - 3(nu_{21} + nu_{03})^2] + \\ (3nu_{21} - nu_{03})(nu_{21} + nu_{03})[3(nu_{30} + nu_{12})^2 - (nu_{21} + nu_{03})^2] \end{aligned} \tag{8}$$

$$I_6 = (nu_{20} - nu_{02})[(nu_{30} + nu_{12})^2 - (nu_{21} + nu_{03})^2] + 4nu_{11}(nu_{30} + nu_{12})(nu_{21} + nu_{03}) \tag{9}$$

$$\begin{aligned} I_7 = (3nu_{21} - nu_{03})(nu_{30} + nu_{12})[(nu_{30} + nu_{12})^2 - 3(nu_{21} + nu_{03})^2] + \\ (3nu_{12} - nu_{30})(nu_{21} + nu_{03})[3(nu_{30} + nu_{12})^2 - (nu_{21} + nu_{03})^2] \end{aligned} \tag{10}$$

The eigenvectors and eigenvalues of the defect were computed from a principal component analysis (PCA) (Wold et al., 1987), which could be useful for distinguishing between the defect with a long axis (branch) and the flatter ones. Furthermore, because of the small number of branches in our

dataset, we did not distinguish between sequential branches and epicormic ones. Nevertheless, the angle between the eigenvector $\overrightarrow{v_1}$ of defect and the trunk axis could be used to classify these types of branch on beech, oak and fir, as epicormic branches were quasi-perpendicular to the trunk axis, while sequential branches were more fastigiated.

2.6.3. Construction of the training dataset

We used both manually segmented and automatically segmented defects to train the random forests. The manual segmentation was done by using a home-made software (DGTalTools-Contrib), based on the library DGTal (DGtal). The software allowed us to select the faces on the mesh to define the footprints of the defects (Figure 5). Each defect was then saved in a separate file and used for training the random forests. We also trained the random forests using the results of our segmentation algorithm, along with the verification given by the shape of paper labels set in the vicinity of the defects and identifiable in the scan. Bark (no-defect) class was introduced even though it is not a defect type; they were bark zones with a roughness higher than the local average. These bark zones are often miss detected as a defect by the segmentation algorithm. This is concordant with our approach as the detection step was built to provide all potential zones of defects assuming the risk of false positive that could be eliminated in the classification step. The training database includes the following classes and the number of defects of each class is summarized in Table 2:

1. Branch, including sequential branch and epicormic branch.
2. Branch scar.
3. Burl.

4. Small defects, including picot, sphaeroblast, bud and bud cluster.

5. Bark.

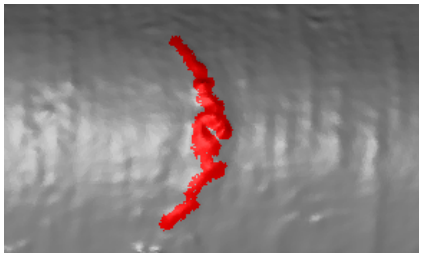

Figure 5: Manual segmentation of a defect

Table 2: Summary of the defects and barks encountered in the training set.

Species	**Branch**	**Branch scar**	**Burl**	**Small defects**	**Bark**
Oak	7	3	159	63	116
Beech	34	51	26	20	2
Wild Cherry	15	5	0	0	0
Pine	0	4	0	0	0
Fir	0	38	0	0	10
Total	56	101	185	83	128

2.6.4. Performance evaluation criteria

To evaluate the performance of the classification algorithm, we used the F-measure, a performance measurement, that is frequently used for classification problems. The F-measure is the harmonic mean of precision (PR) and recall (RE). We used the F_1 score, mixing both with equal weights on PR and RE. The precision PR is the number of correctly classified positive

defects divided by the number of defects labeled by the system as positive (equation (11)). The recall is the number of correctly classified positive defects divided by the number of positive defects in the data (equation (12)). On a binary classification problem, the F_1 is defined by equation (equation (13)).

$$PR = \frac{TP}{TP + FP} \tag{11}$$

$$RE = \frac{TP}{TP + FN} \tag{12}$$

where TP, FP, FN are true positive, false positive and false negative respectively. Their definition is as follows:

- TP is the number of actual defects correctly classified as defect.
- FP is the number of non-defects incorrectly classified as defect.
- FN is the number of actual defects incorrectly classified as non-defect.

$$F_1 = 2\frac{PR.RE}{PR + RE} \tag{13}$$

For a multi-class classification problem, the F-measure must be extended from the binary classification by an average of the F-measure of each class. There are two approaches (Manning et al., 2008). One approach is the macro-averaged F-measure (equation (14)), which is the unweighted mean of F-measure for each label. The other is the micro-averaged F-measure (equation (15)), which considers predictions from all instances together and calculate

the F-measure across all labels. Arithmetically, the micro-averaging favors bigger classes.

$$F_{m1} = \frac{\sum_{i=1}^{n} F_{1i}}{n} \tag{14}$$

$$F_{\mu 1} = 2\frac{PR_{\mu}.RE_{\mu}}{PR_{\mu} + RE_{\mu}} \tag{15}$$

$$PR_{\mu} = \frac{\sum_{i=1}^{n} TP_i}{\sum_{i=1}^{n} (TP_i + FP_i)} \tag{16}$$

$$RE_{\mu} = \frac{\sum_{i=1}^{n} TP_i}{\sum_{i=1}^{n} (TP_i + FN_i)} \tag{17}$$

where n is the number of classes.

We also used the confusion matrix (Provost and Kohavi, 1998) to evaluate the performance for a more detailed analysis of the misclassification between classes.

3. Results

In this section, we present the results of the segmentation algorithm followed by the results of the classification algorithm in comparison with the ground-truth data. We first present a global analysis of the performance related to exhaustiveness independently of the defect type focused on the differences coming from tree species. Then, the analysis of the results focuses on defect types independently of the species which are nevertheless considered in the discussion.

Table 3 shows the results of the segmentation algorithm for each individual tree in the test database in terms of defect detection. We can see that the segmentation algorithm detected almost all of the defects, with 179 detected out of 183 (97.8%) in total. However, the number of false positives was very high (765), which will then be removed by the classification algorithm through a refined analysis of each detected areas. Moreover, Table 3 also shows that these false positives were mostly removed by the classification algorithm at the expense of some defects lost. The classification algorithm removed not only 694 (90.7%) false positives but also 28 (15.3%) actual defects.

We also observed that the segmentation algorithm produced more false positives on trees with furrowed barks, such as oak and pine, than on trees with smooth barks, such as beech and wild cherry. By contrast, the classification algorithm removed the false positives more efficiently on trees with furrowed bark than on trees with smooth-bark. For example, in Table 3, we can see that on pine the number of false positives from the segmentation and classification are 105 and 2 respectively while on Beech 2 these numbers are 70 and 12, respectively. The difference is illustrated in Figure 6.

Table 3: Results of the segmentation (seg.) and classification (cla.) steps compared with the observed defects.

Tree name	**Observed**	**True positive**		**False positive**		**False negative**	
		Seg.	**Cla.**	**Seg.**	**Cla.**	**Seg.**	**Cla.**
Oak 1	8	8	8	9	0	0	0
Oak 2	25	24	19	147	7	1	6
Oak 3	24	23	20	79	7	1	4
Beech 1	30	30	24	55	19	1	6
Beech 2	29	29	21	70	12	0	8
Beech 3	24	22	18	47	14	2	6
Wild Cherry	8	8	8	10	0	0	0
Pine	4	4	4	105	2	0	0
Fir	14	14	14	129	8	0	0
Spruce	17	17	15	114	2	0	4
Total	183	179	151	765	71	5	34

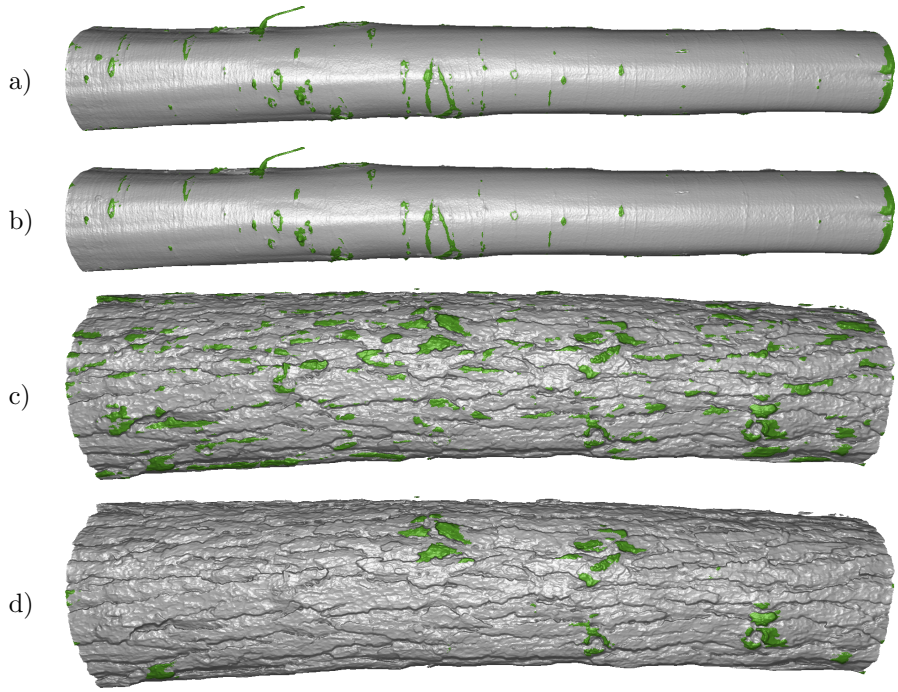

Figure 6: Defects detected by the segmentation algorithm (a, c) and refinement by the classification algorithm (b, d) for two logs: Beech 2 (a, b) and Pine (c, d).

Concerning the performance according to defect types, Figure 7 illustrates classification results by coloring the mesh in agreement with the defect type.

Table 4 shows the performance criteria by defect types resulting from the classification. The overall macro- and micro-averaged scores were 0.86 and 0.73, respectively. However, the algorithm did not perform equally well on all classes of defect. The branch had the best F_1 score of 0.89, followed by the burl with an F_1 score of 0.76. The algorithm performed less well on branch scar and the small defect types with F_1 scores of 0.61 and 0.46, respectively.

For allowing a better understanding of the differences, Figure 8 represents the confusion matrix of the classification result. The matrix shows the match-

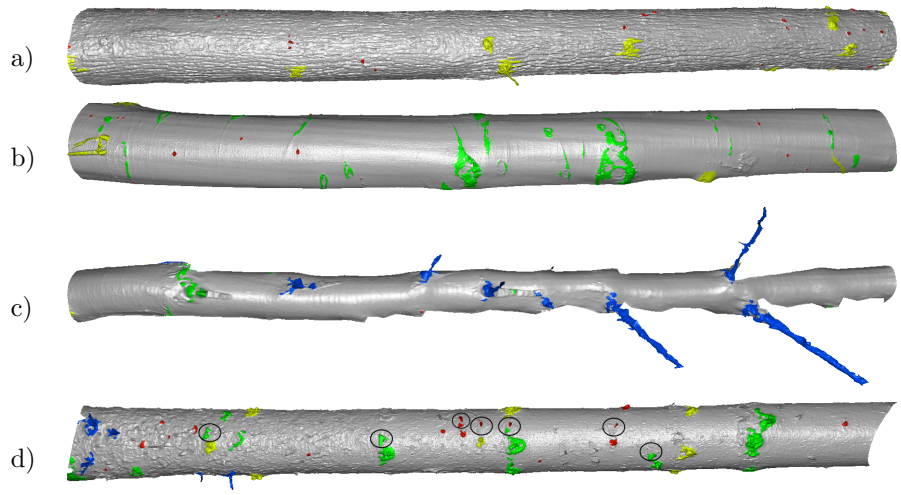

Figure 7: Examples of the classification results on the mesh of Oak 3 (a), Beech 1 (b), Wild cherry 3 (c), and Spruce (d). is **Branch** type including both sequential and epicormic branches, is **Branch scar**, is Burl, is **Small defect** including bud cluster, sphaeroblast and picot. On the mesh of the Spruce, the detected defects (circled) are the paper marks and pushpins that were used by the expert to mark the defect type before the scan was carried out. These false positives were ignored in our evaluation.

ing between predicted and observed defect types and allows a finer analysis of the differences. We can see that one branch was classified as branch scar. A more detailed analysis showed that it was a short dead stub branch of a wild cherry (the large green region in Figure 7 (c)). Another branch was classified as a burl because an epicormic branch is often originated from a small burl, and the distinction by the algorithm is difficult in young development stages. While the recall of the algorithm on the branch scar was very high (0.84), the precision was not as good (0.48) because there were 49 bark portions recognized as branch scar while there were 69 branch scars in total. Some burls were confounded with the bark portions and small defects be-

Table 4: Precision, recall and F_1 score of the different defect types

Defect type	**Precision**	**Recall**	F_1
Branch	1.00	0.80	0.89
Branch scar	0.48	0.84	0.61
Burl	0.73	0.81	0.76
Small defect	0.56	0.39	0.46
Bark	0.95	0.90	0.93
Beech (micro avg.)	0.70	0.70	0.70
Beech (macro avg.)	0.70	0.70	0.70
Oak (micro avg.)	0.90	0.90	0.90
Oak (macro avg.)	0.66	0.68	0.67
All (micro avg.)	0.86	0.86	0.86
All (macro avg.)	0.75	0.74	0.73

cause a burl consisting of only buds may have a similar look to a small defect (see Figure 1 (i) and (j)) or a bark portion since both are quite flat. The confusion matrix shows that the small defects were often confounded with bark portions and branch scars. It is to be noted that the number of bark portions miss-classified as small defects was 15 and the number of small defects miss-classified as bark portions was 16. There was only one branch scar miss-classified as small defect but 11 small defects miss-classified as branch scars.

Although no spruce data were used to train the random forests, the predictions on this spruce (Figure 7 (d)) were good, as 15 out of 18 were detected. However, two branch scars were detected as small defects and two branch

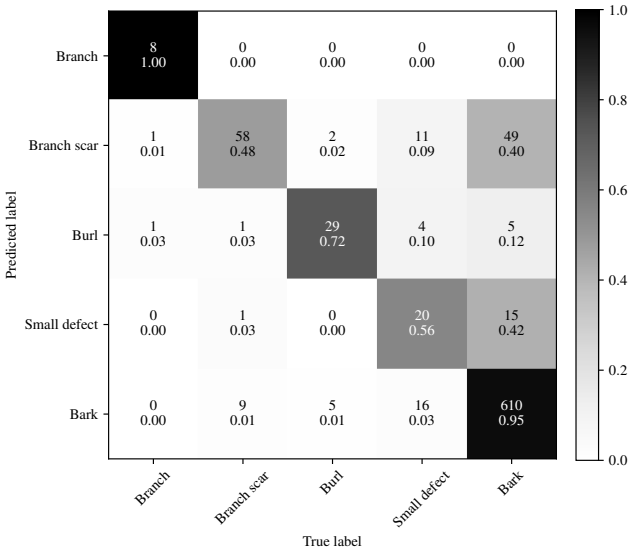

Figure 8: Confusion matrix with the absolute value and normalized value (precision). The color of cells is a function of normalized value.

scars were detected as burls.

4. Discussion

4.1. Defect detection

In summary, our algorithms had a very good performance in defect detection, even with the small defects corresponding to a slight modification of the bark roughness. These good results are both due to the robust estimation of the trunk centerline, and the fitting on a local longitudinal patch, of the regular radius variation, allowing for the calculation a local reference distance. Our approach outperforms the detection based on a radius resulting from the fitting of geometrical primitives such as circle or cylinders proposed in other works (Thomas et al., 2007; Kretschmer et al., 2013) especially for cross-sections with less circular shape as already discussed in Nguyen et al.

(2016b). It is clear that several factors can impact the detection, such as scan resolution and quality and missing data resulting from occlusion. Our algorithm can detect small defects such as picot which often have a diameter between 0.5 centimeter and 1 centimeter, thus outperforming all previous works with size ranging from 7.5 centimeters (Thomas et al., 2007) to 2.0 centimeters (Kretschmer et al., 2013). Moreover, Kretschmer et al. (2013) only focused on the branch scars and their method was not automatic.

Because of their shapes, French and North American foresters have named large branch scars of beech and wild cherry trees "Chinese mustache" (or eyebrow). It often covers a large peripheral area, and the two parts of the mustache are often thin. This may result in an over-segmentation (Figure 9 (a)). Two or more large defects can also be close enough to form a large shape. Although the human eye will dissociate the large shape as multiple separated defects, the algorithm saw it as a defect, which consequently created an under-segmentation (Figure 9 (b)). The under-segmentation can also occur on the trunk of conifer in the case of connected branch scars (Figure 9 (c)).

(a) (b) (c)

Figure 9: Examples of over-segmentation on beech (a), under-segmentation on beech (b) and on spruce (c). Within each image, all connected green areas belong to the same defect.

As the segmentation is the step preceding the classification, the perfor-

mance of the classification algorithm also depends on the performance of the segmentation step. Thus, any improvement in segmentation will result in a better classification. The most important parameters were the patch size and the bin width of the histogram used to find the threshold by the Rosin's method (Rosin, 2001), and the voxel size used to compute the centerline. Their choices were described in detail in Nguyen et al. (2016a). As mentioned earlier, the over and under-segmentation can occur in the segmentation step especially through the defect clustering through a Euclidean distance filter. These errors can affect the classification, and consequently, the assessment of the tree quality. In addition to the influence of misclassification, the over-segmentation increased the number of defects and decreased their dimension. By contrast, the under-segmentation decreased the number of defects and increased their dimensions.

4.2. Defect classification

Visually, we can see that our algorithms were able to detect and classify most of the defects (Figure 7), including small defects such as picot and bud clusters. Based on Table 4, the overall classification result was good, with a micro-averaged F_1 score of 0.86 and a macro-averaged score of 0.73. The result was promising, particularly on the classification of branch and burl. However, we did not obtain a very high F_1 score (0.46) on the small defect because, first, we could not totally remove all the false positives and, second, there was some confusion between the classes due to the very high intra-class variability and the interclass similarity.

For example, the confusion between branch scars and burls can be explained by the fact that some burls containing only buds have a shape that

looks like a branch scar because both are flat. In the field, human eyes can easily distinguish these two defect types; however, in the point cloud or mesh, it could be difficult to distinguish them. For small-sized defects, the confusion between burls and small defects can merely be explained by the initial definition of burl and small defect. When a burl is composed only of buds it might have a similar shape to a bud cluster. In our database, small defect types include several biological defect types: a bud cluster with less than six buds, sphaeroblast, and picot. A bud cluster may have a shape similar to a small burl. The confusion was high, even for expert eyes.

With the objective of wood quality assessment, subclasses considering the size of defects with the same biological origin can be useful to refine the analysis in future studies but need a suitable assessment of the defect characteristics by algorithms, which is beyond the scope of this paper. More generally, it addresses the problem of a combination of defects that occurs rather frequently because they have the same origin and correspond to different stages of development or because they result from a spatial proximity, as in examples illustrating under-segmentation in Figure 9. Improvements could be a more refined algorithm for merging close protruding areas and a detailed definition of the defect types, adding size classes linked to the resulting quality impact as already mentioned.

4.2.1. Influence of species and bark roughness

As a non-intuitive result (coming from the easier visual assessment of the defects on smooth bark), a lower F_1 score was observed on beech compared with oak (Table 4). In the segmentation step, on trees with furrowed bark, there were many more false positives, resulting of the misdetection of bark

portions as defects. This is in agreement with our hypothesis. However, the false positives on trees with furrowed bark had a common shape created by the pattern of the rhytidome, and they were easily detectable and removed by the classification through the definition of the Bark class. In contrast, on trees with smooth bark, the false positives were created by bark portions, very similar to actual defects in terms of protrusion and spatial distribution. Moreover, on species with smooth bark, and particularly on beech, we also observed many wrinkles or cambium alterations revealed by the elliptical shape (*Nectria* disease) of bark (Figure 10). These alterations were often misclassified by our algorithm as branch scars rather logically in the absence of more relevant type definition corresponding to these singularities. Thus, the classification algorithm has a higher performance on furrowed bark trees than on smooth bark trees.

4.2.2. Parameters of random forests and future improvements

Random forests have only two principal parameters: the number of trees in the forest ($nbTrees$) and the number of variables ($nbVariables$) used to select and test for the best split when growing the trees. Their performance was slightly influenced by the number of trees if it was chosen sufficiently high (1,000 trees in our experiment). With the number of trees over 1,000, the performance gain was minimal. $nbVariables$ was chosen following the OpenCV recommendation, which was $\sqrt{variables}$. We also noticed that random forests are very robust to over-fitting so the feature selection is less critical. Random forests can give a good performance, even with a small training dataset (Rodriguez-Galiano et al., 2012); however, it depends also on the intra-class variability of the defect class. Because burl and branch scar

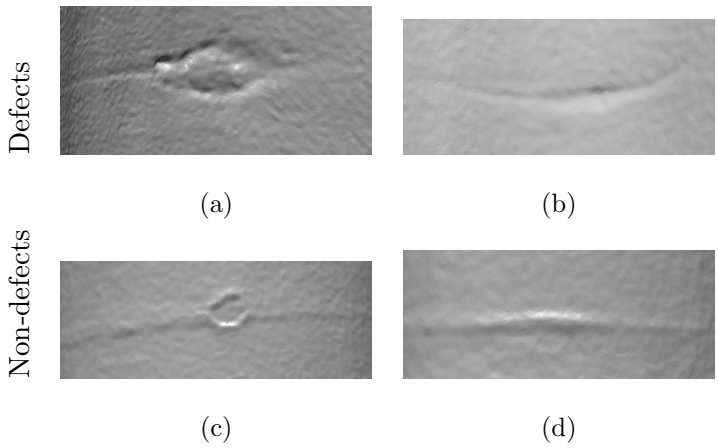

Figure 10: Examples of equivalent bark appearances considered either to be a branch scar ((a) and (b)) or a non-defect ((c) and (d)). This has been determined according to our own biological expertise. This figure illustrates the difficulty distinguish between defects and non-defects. The region in (c), while having a shape similar to a branch scar as in (a), is a scar resulting from slight damages due to *Nectria* attack affecting just the bark and not the wood below. The region in (d) has been considered as non-defect since it was formed by the covering of a dead bud during the very first years of tree development with no consequence for the wood quality.

have a high intra-class variability, in future work, we would like to add more training data of these types. As the incident angle of laser beams changes with the different heights of the trunk, it is also important to have the defect data from different trunk heights.

Another suggestion to improve the performance of the classification is to remove species in the feature vector and separately train random forests for each species, considering that the information on the species is a prerequisite brought by an operator or by another identification step (Othmani et al., 2013). This approach might have a better performance but requires more

training data. Our test carried out with data of the most present species (beech) in our database did not clearly outperform random forests trained with all species. The $F_{\mu 1}$ were 0.71 for random forests trained with only beech defects and 0.70 for random forests trained with all species defects.

4.3. Use for grading trunk quality

The performance of defect classification can influence the grading result of standing trees. Nonetheless, the impact of the misclassification of class on the quality assessment is difficult to assess. The most important is the classification of large defects. Once there is an occurrence of these large defects, the occurrence of smaller defects is less important. However, in the case of highest quality trunk, the classification performance is more critical because one misclassification, even of a small defect, can result in a change to a higher or lower quality class. Thus, a further development of the current method is needed to measure the defect dimension which is required to assess the impact of defects by a standard (AFNOR, 1999a,b, 2012).

Regarding the current scanning setting, the spatial resolution does not allow for classifying between a picot and a less important small defect, such as bud cluster. Only one picot is allowed in the case of highest quality trunk. Thus, in the case that there is only the occurrence of small defects, an additional expert inspection could be suggested to verify the classification result in the case of high commercial value. Beyond grading issues, the information about defect type and position on the log can be used to optimize the transformation, with the objective of increasing the volume of high-quality products but such exceeds the scope of this paper even if it is a real prospect.

As a common problem for the remote sensing technologies, the quality of

TLS data can be limited by the occlusion, especially when there are branches on the trunk or false positive created by moss (*Musci L.*) or lichens. In general, scanning the tree from multiple views can reduce occlusions, as the occlusion on the high part of the tree is difficult to avoid.

5. Conclusions

In this paper, we have presented a random forests-based classifier to identify defects on trunk surface from TLS data. The potential defects were detected by our segmentation algorithm (Nguyen et al., 2016b). Each detected defect was then classified into one of the four defect classes or bark using the random forests classifier. Our experiment showed that from the high-density data acquired by TLS, we can detect and classify most of the defects on tree bark. The overall $F_{\mu 1}$ score of the classification algorithm was 0.86. These preliminary results are thus very promising. We could further improve the score with the addition of more data and with the definition of defect subclasses considering not only their biological type but also their size and impact on wood quality. An interesting option will be to train the random forests separately for each tree species. The information about the defect type in addition to its dimension and position can be used to assess the quality of roundwood or standing tree. This is the first step towards developments for helping experts in the assessment of the quality of standing trees or timber logs in forests or for enhancing the knowledge coming from true shape scanners in the primary wood processing industry.

Acknowledgments

This work was supported by the French National Research Agency through the Laboratory of Excellence ARBRE (ANR-12-LABXARBRE-01) and by the Lorraine French Region. We would like to thank Florian Vast for providing technical support and for scanning and measuring the trees used in this research.

References

AFNOR, 1999a. EN 1927-1 - Classement qualitatif des bois ronds résineux - Partie 1 : épicéas et sapins
Qualitative classification of softwood round timber - Part 1 : Spruces and firs.

AFNOR, 1999b. EN 1927-2 - Classement qualitatif des bois ronds résineux - Partie 2 : pins
Qualitative classification of softwood round timber - Part 2 : Pines.

AFNOR, 2012. EN 1316-1 - Bois ronds feuillus - Classement qualitatif - Partie 1: Chêne et hêtre
Hardwood round timber - Qualitative classification - Part 1: Oak and beech.

Aguilera, C., Sanchez, R., Baradit, E., 2008. Detection of knots using X-ray tomographies and deformable contours with simulated annealing. Wood Res. 53, 57–66.

726 Astrup, R., Ducey, M.J., Granhus, A., Ritter, T., von Lüpke, N., 2014.
727 Approaches for estimating stand-level volume using terrestrial laser scan-
728 ning in a single-scan mode. Can. J. For. Res 44, 666–676. doi:10.1139/
729 cjfr-2013-0535.

730 Bishop, C.M., 1995. Neural Networks for Pattern Recognition. Oxford Uni-
731 versity Press, Inc., New York, NY, USA.

732 Blanchette, D., Fournier, R.A., Luther, J.E., Côté, J.F., 2015. Predicting
733 wood fiber attributes using local-scale metrics from terrestrial lidar data:
734 A case study of newfoundland conifer species. For. Ecol. Manage. 347, 116
735 – 129. doi:10.1016/j.foreco.2015.03.013.

736 Boltcheva, D., Lévy, B., 2017. Surface reconstruction by computing restricted
737 voronoi cells in parallel. Computer-Aided Design 90, 123–134. doi:10.
738 1016/j.cad.2017.05.011.

739 Bradski, G., 2000. The OpenCV Library. Dr. Dobb's Journal of Software
740 Tools .

741 Breiman, L., 2001. Random forests. Mach. Learn. 45, 5–32. doi:10.1023/A:
742 1010933404324.

743 Breiman, L., Friedman, J., Stone, C.J., Olshen, R.A., 1984. Classification
744 and regression trees. Wadsworth Int Group, Belmont, CA.

745 Chehata, N., Guo, L., Mallet, C., 2009. Airborne lidar feature selection for
746 urban classification using random forests. Int. arch. photogramm. remote
747 sens. spat. inf. sci. 38, 207–212.

748 Colin, F., Mechergui, R., Dhôte, J.F., Fontaine, F., 2010a. Epicormic on-
749 togeny on quercus petraea trunks and thinning effects quantified with the
750 epicormic composition. Ann. For. Sci. 67, 813–813. doi:10.1051/forest/
751 2010049.

752 Colin, F., Mothe, F., Freyburger, C., Morisset, J.B., Leban, J.M., Fontaine,
753 F., 2010b. Tracking rameal traces in sessile oak trunks with X-ray computer
754 tomography: Biological bases, preliminary results and perspectives. Trees-
755 Struc. Func. 24, 953–967. doi:10.1007/s00468-010-0466-1.

756 Cortes, C., Vapnik, V., 1995. Support-vector networks. Mach. Learn. 20,
757 273–297. doi:10.1007/BF00994018.

758 Dassot, M., Colin, A., Santenoise, P., Fournier, M., Constant, T., 2012.
759 Terrestrial laser scanning for measuring the solid wood volume, includ-
760 ing branches, of adult standing trees in the forest environment. Comput.
761 Electron. Agric. 89, 86 – 93. doi:10.1016/j.compag.2012.08.005.

762 Dassot, M., Constant, T., Fournier, M., 2011. The use of terrestrial lidar
763 technology in forest science: Application fields, benefits and challenges.
764 Ann. For. Sci. 68, 959–974. doi:10.1007/s13595-011-0102-2.

765 Devroye, L., Györfi, L., Lugosi, G., 1996. A Probabilistic Theory of Pat-
766 tern Recognition. Springer New York, New York, NY. doi:10.1007/
767 978-1-4612-0711-5.

768 DGtal, . DGtal: Digital Geometry tools and algorithms library. http:
769 //dgtal.org.

770 Díaz-Uriarte, R., De Andres, S.A., 2006. Gene selection and classification of
771 microarray data using random forest. BMC Bioinform. 7. doi:10.1186/
772 1471-2105-7-3.

773 Fink, S., 1999. Pathological and Regenerative Plant Anatomy. Schweizerbart
774 Science Publishers, Stuttgart, Germany.

775 Fonseca, M.A., 2005. The measurement of roundwood: methodologies and
776 conversion ratios. CABI Publishing, Wallingford, Oxfordshire, UK.

777 Gardiner, B., Moore, J., 2014. Creating the wood supply of the fu-
778 ture, in: Fenning T. (eds) Challenges and Opportunities for the World's
779 Forests in the 21st Century. Springer, pp. 677–704. doi:10.1007/
780 978-94-007-7076-8_30.

781 Gislason, P., Benediktsson, J., Sveinsson, J., 2006. Random forests for land
782 cover classification. Pattern Recognit. Lett. 27, 294–300. doi:10.1016/j.
783 patrec.2005.08.011.

784 Guo, L., Chehata, N., Mallet, C., Boukir, S., 2011. Relevance of airborne lidar
785 and multispectral image data for urban scene classification using random
786 forests. ISPRS J. Photogramm. Remote Sens. 66, 56–66. doi:10.1016/j.
787 isprsjprs.2010.08.007.

788 Hopkinson, C., Chasmer, L., Young-Pow, C., Treitz, P., 2004. Assessing
789 forest metrics with a ground-based scanning lidar. Can. J. For. Res 34,
790 573–583. doi:10.1139/x03-225.

791 Hu, M.K., 1962. Visual pattern recognition by moment invariants. IRE

Transactions on Information Theory 8, 179–187. doi:10.1109/TIT.1962.1057692.

Kankare, V., Joensuu, M., Vauhkonen, J., Holopainen, M., Tanhuanpää, T., Vastaranta, M., Hyyppä, J., Hyyppä, H., Alho, P., Rikala, J., et al., 2014. Estimation of the timber quality of scots pine with terrestrial laser scanning. Forests 5, 1879–1895. doi:10.3390/f5081879.

Krähenbühl, A., Kerautret, B., Debled-Rennesson, I., Longuetaud, F., Mothe, F., 2012. Knot detection in X-ray CT images of wood, in: International Symposium on Visual Computing, Springer. pp. 209–218. doi:10.1007/978-3-642-33191-6_21.

Krähenbühl, A., Roussel, J.R., Kerautret, B., Debled-Rennesson, I., Mothe, F., Longuetaud, F., 2016. Robust knot segmentation by knot pith tracking in 3d tangential images, in: International Conference on Computer Vision and Graphics, Springer. pp. 581–593. doi:10.1007/978-3-319-46418-3_52.

Kretschmer, U., Kirchner, N., Morhart, C., Spiecker, H., 2013. A new approach to assessing tree stem quality characteristics using terrestrial laser scans. Silva Fenn. 47, 1–14. doi:10.14214/sf.1071.

Lévy, B., Bonneel, N., 2013. Variational anisotropic surface meshing with voronoi parallel linear enumeration, in: Proceedings of the 21st international meshing roundtable. Springer, pp. 349–366. doi:10.1007/978-3-642-33573-0-21.

Li, P.L.P., a.L. Abbott, Schmoldt, D., 1996. Automated analysis of CT images for the inspection of hardwood logs, in: Proceedings of International Conference on Neural Networks (ICNN'96), IEEE. pp. 1744–1749. doi:10.1109/ICNN.1996.549164.

Lin, W., Wang, J., 2012. An integrated 3D log processing optimization system for hardwood sawmills in central Appalachia, USA. Comput. Electron. Agric. 82, 61–74. doi:10.1016/j.compag.2011.12.014.

Longuetaud, F., Mothe, F., Kerautret, B., Krähenbühl, A., Hory, L., Leban, J., Debled-Rennesson, I., 2012. Automatic knot detection and measurements from X-ray CT images of wood: A review and validation of an improved algorithm on softwood samples. Comput. Electron. Agric. 85, 77 – 89. doi:10.1016/j.compag.2012.03.013.

Luther, J.E., Skinner, R., Fournier, R.A., van Lier, O.R., Bowers, W.W., Coté, J.F., Hopkinson, C., Moulton, T., 2014. Predicting wood quantity and quality attributes of balsam fir and black spruce using airborne laser scanner data. Forestry 87, 313–326. doi:10.1093/forestry/cpt039.

Maltamo, M., Peuhkurinen, J., Malinen, J., Vauhkonen, J., Packalén, P., Tokola, T., et al., 2009. Predicting tree attributes and quality characteristics of scots pine using airborne laser scanning data. Silva Fenn. 43, 507–521.

Manning, C.D., Raghavan, P., Schütze, H., 2008. Introduction to Information Retrieval. Cambridge University Press. chap-

836 ter 13. p. 280. URL: https://nlp.stanford.edu/IR-book/
837 information-retrieval-book.html, doi:10.1017/CBO9780511809071.

838 Microtec, 2019. CT Log. URL: https://microtec.eu/en/catalogue/
839 products/ctlog. Last visited on 2019/02/10.

840 Müller, F., Jaeger, D., Hanewinkel, M., 2019. Digitization in wood supply –
841 A review on how Industry 4.0 will change the forest value chain. Comput.
842 Electron. Agric. 162, 206–218. doi:10.1016/j.compag.2019.04.002.

843 Mutanga, O., Adam, E., Cho, M.A., 2012. High density biomass estima-
844 tion for wetland vegetation using worldview-2 imagery and random for-
845 est regression algorithm. Int. J. Appl. Earth Obs. Geoinf. 18, 399–406.
846 doi:10.1016/j.jag.2012.03.012.

847 Nguyen, V.T., Kerautret, B., Debled-Rennesson, I., Colin, F., Piboule,
848 A., Constant, T., 2016a. Algorithms and implementation for segment-
849 ing tree log surface defects, in: International Workshop on Reproducible
850 Research in Pattern Recognition, Springer. pp. 150–166. doi:10.1007/
851 978-3-319-56414-2_11.

852 Nguyen, V.T., Kerautret, B., Debled-Rennesson, I., Colin, F., Piboule, A.,
853 Constant, T., 2016b. Segmentation of defects on log surface from terres-
854 trial lidar data, in: Pattern Recognition (ICPR), 2016 23rd International
855 Conference on, IEEE. pp. 3168–3173. doi:10.1109/ICPR.2016.7900122.

856 Niemeyer, J., Rottensteiner, F., Soergel, U., 2014. Contextual classification
857 of lidar data and building object detection in urban areas. ISPRS J. Pho-

858 togramm. Remote Sens. 87, 152–165. doi:10.1016/j.isprsjprs.2013.
859 11.001.

860 Othmani, A., Voon, L.F.L.Y., Stolz, C., Piboule, A., 2013. Single tree species
861 classification from terrestrial laser scanning data for forest inventory. Pat-
862 tern Recognit. Lett. 34, 2144–2150. doi:10.1016/j.patrec.2013.08.004.

863 Pickens, J.B., Throop, S.A., Frendewey, J.O., 1997. Choosing Prices to
864 Optimally Buck Hardwood Logs with Multiple Log-Length Demand Re-
865 strictions. For. Sci. 43, 403–413. doi:10.1093/forestscience/43.3.403.
866 publisher: Narnia.

867 Provost, F., Kohavi, R., 1998. Glossary of terms. journal of machine learning
868 30, 271–274. doi:10.1023/A:1017181826899.

869 Pyörälä, J., Kankare, V., Vastaranta, M., Rikala, J., Holopainen, M., Sipi,
870 M., Hyyppä, J., Uusitalo, J., 2018. Comparison of terrestrial laser scanning
871 and X-ray scanning in measuring Scots pine (Pinus sylvestris L.) branch
872 structure. Scand. J. For. Res. 33, 291–298. doi:10.1080/02827581.2017.
873 1355409.

874 Racko, V., 2013. Verify the accurancy of estimation the model between
875 dimensional characteristics of branch scar and the location of the knot in
876 the beech trunk. Annals of Warsaw Univ. of Life Sciences-SGGW. Forestry
877 & Wood Technology 84.

878 Jörg Elektronik GmbH, 2019. JORO-X: X-ray scanner - Detection of internal
879 wood qualities. URL: https://www.je-gmbh.de/en/Products/JORO-X.
880 Last visited on 2019/02/10.

881 Rodriguez-Galiano, V.F., Ghimire, B., Rogan, J., Chica-Olmo, M., Rigol-
882 Sanchez, J.P., 2012. An assessment of the effectiveness of a random forest
883 classifier for land-cover classification. ISPRS J. Photogramm. Remote Sens.
884 67, 93–104. doi:10.1016/j.isprsjprs.2011.11.002.

885 Rosin, P.L., 2001. Unimodal thresholding. Pattern Recognit. 34, 2083–2096.
886 doi:10.1016/S0031-3203(00)00136-9.

887 Schütt, C., Aschoff, T., Winterhalder, D., Thies, M., Kretschmer, U.,
888 Spiecker, H., 2004. Approaches for recognition of wood quality of standing
889 trees based on terrestrial laserscanner data, in: Proceedings of the IS-
890 PRS working group VIII/2, Freiburg, Germany. International Archives of
891 Photogrammetry, Remote Sensing, and Spatial Information Sciences, pp.
892 179–182.

893 Simonse, M., Aschoff, T., Spiecker, H., Thies, M., 2003. Automatic de-
894 termination of forest inventory parameters using terrestrial laserscanning,
895 in: Proceedings of the ScandLaser Scientific Workshop on Airborne Laser
896 Scanning of Forests, pp. 252–258.

897 Stängle, S.M., Brüchert, F., Kretschmer, U., Spiecker, H., Sauter, U.H., 2014.
898 Clear wood content in standing trees predicted from branch scar measure-
899 ments with terrestrial lidar and verified with X-ray computed tomography
900 1. Can. J. For. Res 44, 145–153. doi:10.1139/cjfr-2013-0170.

901 Terzopoulos, D., Fleischer, K., 1988. Deformable models. Vis Comput. 4,
902 306–331. doi:10.1007/BF01908877.

Thomas, L., Shaffer, C.A., Mili, L., Thomas, E., 2007. Automated detection of severe surface defects on barked hardwood logs. For. Prod. J. 57, 50–56.

Thomas, L., Thomas, R.E., 2010. A graphical automated detection system to locate hardwood log surface defects using high-resolution three-dimensional laser scan data, in: Proceedings of the 17th Central Hardwood Forest Conference, pp. 92–101.

Thomas, R.E., 2009. Modeling the relationships among internal defect features and external Appalachian hardwood log defect indicators. Silva Fenn. 43, 447–456.

Van Leeuwen, M., Hilker, T., Coops, N.C., Frazer, G., Wulder, M.A., Newnham, G.J., Culvenor, D.S., 2011. Assessment of standing wood and fiber quality using ground and airborne laser scanning: a review. For. Ecol. Manage. 261, 1467–1478. doi:10.1016/j.foreco.2011.01.032.

Van Leeuwen, M., Nieuwenhuis, M., 2010. Retrieval of forest structural parameters using lidar remote sensing. Eur. J. For. Res. 129, 749–770. doi:10.1007/s10342-010-0381-4.

Wold, S., Esbensen, K., Geladi, P., 1987. Principal component analysis. Chemom. Intell. Lab. Syst 2, 37–52. doi:10.1016/0169-7439(87)80084-9.

Yao, T., Yang, X., Zhao, F., Wang, Z., Zhang, Q., Jupp, D., Lovell, J., Culvenor, D., Newnham, G., Ni-Meister, W., et al., 2011. Measuring forest structure and biomass in New England forest stands using echidna ground-based lidar. Remote Sens. Environ. 115, 2965–2974. doi:10.1016/j.rse.2010.03.019.

926 Yuan, F., Sawaya, K.E., Loeffelholz, B.C., Bauer, M.E., 2005. Land
927 cover classification and change analysis of the Twin Cities (Minnesota)
928 Metropolitan Area by multitemporal Landsat remote sensing. Remote
929 Sens. Environ. 98, 317–328. doi:10.1016/j.rse.2005.08.006.

930 Zhu, D., Conners, R.W., Schmoldt, D.L., Araman, P.a., 1996. A prototype
931 vision system for analyzing CT imagery of hardwood logs. IEEE Trans.
932 Syst. Man. Cybern. B Cybern. 26, 522–532. doi:10.1109/3477.517028.